Episomal virus maintenance enables bacterial population recovery from infection and virus-bacterial coexistence

Rodrigo Sanchez-Martinez[1]*, Akash Arani[2]*, Mart Krupovic[3], Joshua S. Weitz[2,4,5]**, Fernando Santos[1,7], Josefa Anton[1,6,7]**

Affiliations

[1] Department of Physiology, Genetics and Microbiology, University of Alicante, San Vicent del Raspeig, Alicante, Spain

[2] Department of Biology, University of Maryland, College Park, MD, USA

[3] Institut Pasteur, Université Paris Cité, Archaeal Virology Unit, Paris, France

[4] Department of Physics, University of Maryland, College Park, MD, USA

[5] Institut de Biologie, École Normale Supérieure, Paris, France

[6] Multidisciplinary Institute of Environmental Studies Ramon Margalef, Alicante, Spain

[7] Institute of Health and Biomedical Research of Alicante (ISABIAL), Alicante, Spain

* These authors contributed equally

** Corresponding authors: jsweitz@umd.edu; anton@ua.es

ABSTRACT

Hypersaline environments harbor the highest concentrations of virus-like particles (VLPs) reported for aquatic ecosystems. The substantial densities of both microbial populations and VLPs challenge traditional explanations of top-down control exerted by viruses. At close to saturation salinities, prokaryotic populations are dominated by *Archaea* and the bacterial clade *Salinibacter*. In this work we examine the episomal maintenance of a virus within a *Salinibacter ruber* host. We found that infected cultures of *Sal. ruber* M1 developed a population-level resistance and underwent systematic and reproducible recovery post infection that was counter-intuitively dependent on the multiplicity of infection (MOI), where higher MOI led to better host outcomes. Furthermore, we developed a nonlinear population dynamics model that successfully reproduced the qualitative features of the recovery. This suggests that the maintenance of the virus episomally, often referred to as pseudolysogeny, and lysis inhibition allow for host-virus co-existence under high MOI infections. Our results emphasize the ecological importance of exploring a spectrum of viral infection strategies beyond the conventional binary of lysis or lysogeny.

INTRODUCTION

Diverse microorganisms adapted to life at high salt concentrations are found in globally distributed hypersaline environments that comprise ~50% of continental waters (1). The abundance of prokaryotes increases with salinity, reaching values even higher than 10^8 cells per milliliter at salinities above 25% (2, 3, 4). The microbial communities in these environments, especially at extreme salinities, are dominated by members of the domain *Archaea* along with *Bacteria* predominantly from the *Salinibacter* clade (5, 6). Amongst bacterial clades, *Salinibacter ruber* was the first bacterium confirmed to grow actively in extreme salinities (7). Global-scale biogeographic studies have revealed that *Sal. ruber* is one of the most prevalent and dispersed bacterial lineages in hypersaline environments. Moreover, it is also characterized by a high intraspecific diversity, which can be caused as a response to an intense viral predation (8, 9, 10). At saturated salt conditions, hypersaline environments are also characterized by the presence of viral-like particles (VLP) that can reach up to 10^{10} VLP/ml (11), more than three orders of magnitude higher than estimates from surface marine communities (12, 13). Measured ratios of

58 viruses to microbes increase with salinity (from seawater to highly salt-saturated ponds) with
59 values between 10 and 100 VLPs per cell, and can even reach 300 VLPs per cell (14). Hypersaline
60 environments at close-to-saturation salinities are typically inhospitable to bacterivorous organisms
61 found in other aquatic habitats, including protists and heterotrophic nanoflagellates (15, 16, 17).
62 Unusually high viral abundances and virus-to-cell ratios along with reduced bacterivory in
63 hypersaline environments suggest that viral infections and the subsequent modulation of microbial
64 cell fate have a significant role in shaping prokaryotic population dynamics (18).

65 At the cellular scale, viral infections can lead to a continuum of outcomes spanning pathways that
66 lead to rapid lysis as well as long-term persistence via lysogeny (19). In the lytic pathway, the
67 virus redirects host metabolism to replicate the viral genome, produce virions, and lyse the host
68 cell, thereby releasing viral progeny to the environment. In the lysogenic pathway, the infecting
69 viral genome replicates along with the host chromosome. The provirus (i.e., the integrated viral
70 genome) can reactivate stochastically or in response to changes in host state, re-initiating the lytic
71 pathway leading to the release of virus particles (20, 21). Viral life cycles span the continuum
72 between these archetypes, including life cycles such as chronic infections, in which there is a
73 progressive release of virions into the environment without cell lysis (22). Another alternative viral
74 life cycle is pseudolysogeny, in which genomes of non-temperate viruses persist inside host cells
75 without integration as episomes, do not replicate synchronously with their host cell, and are
76 transmitted asymmetrically from mother to daughter cells (23, 24).

77 The presence of high microbial densities, low bacterivory, and unusually high VLP levels in
78 saturated brines presents a challenge to conventional explanations of top-down control. If
79 extremely high viral densities are achieved through efficient infection and lysis, one might expect
80 strong selection for viral-resistance via Kill-the-Winner like mechanisms (25, 26) or even the local
81 collapse of archaeal and bacterial communities (and their viruses) until recolonized via dispersal.
82 Alternatively, prokaryotes and viruses may persist at high levels in hypersaline environments
83 because of sustained production from infected cells or a high stability of non-infectious viruses.
84 Here, we utilize a *Sal. ruber*-virus model system to explore the mechanistic basis for the
85 persistence and coexistence of high-density populations of viruses and bacterial hosts in
86 hypersaline environments. Initial experiments revealed that virus infections led to a transient
87 bacterial population crash followed by a recovery. However, contrary to our expectations and

leveraging a combination of experiments, sequencing, and mathematical modeling, we conclude that bacterial population recovery was not enabled by the emergence of virus-resistant bacterial mutants or lysogeny. Instead, bacterial population recovery was enabled via the initiation of a persistent infection characterized by the episomal maintenance of viruses that protected infected cells from subsequent infection and lysis. As we show, this persistent infection enables lytic viruses to persist at high abundances without necessarily eliminating their hosts, providing new challenges to paradigms of virus-microbe coexistence in extreme environments.

RESULTS

Systematic and reproducible recovery of *Sal. ruber* populations after viral-induced lysis

We infected *Sal. ruber* strain M1 with the virulent M1EM-1 virus (27) (named henceforth EM1 for convenience) at a MOI=0.01 in triplicate at time=0 h (Fig. 1a). In all three replicates, we observed a rapid stabilization in the host optical density (OD) following infection due to lysis, followed by a population-level recovery at 80 h such that infected cultures eventually recovered to the levels comparable to those of the virus-free control, reaching the stationary state ODs (see Methods for further details). This systematic recovery of the population post infection was also observed in other *Sal. ruber*-virus pairs (see Extended Data Fig. 1). This finding was unexpected as the EM1 virus does not encode lysogenic markers (i.e., excisionases and integrases) which would allow its integration into the host chromosome, facilitating superinfection exclusion-mediated population level recovery as seen for some temperate viruses (28). We further examined this recovery phenomenon by infecting *Sal. ruber* M1 with the EM1 virus at ten-fold higher viral levels (MOI=0.1) and using more replicates (10 replicates for both control and infection treatment; Fig. 1b). In this case, we observed a sharp decrease in the OD levels of the infected cultures, consistent with the 10x increase in viral pressure (MOI=0.1 vs. MOI=0.01). However, we once again observed recovery dynamics comparable in all ten replicates.

Sal. ruber recovery is not consistent with the proliferation of virus-resistant mutants or the integration of viral genomes into bacterial genomes

115 We hypothesized that reproducible recovery of infected cell cultures is not caused by spontaneous
116 mutations and the emergence and proliferation of virus-resistant bacterial populations which
117 typically involves jackpot like variability that is incompatible with the observed reproducibility in
118 recovery times (29). Nonetheless, to assess the link between recovery and virus-resistance, all
119 replicates (both the infected cultures and the controls) from the recovered cultures shown in Fig.
120 1a (named C_F) were sequenced. The initial *Sal. ruber* M1 used as a host (named C_0) was also
121 sequenced as a control. We then analyzed and compared the sequenced genomes to evaluate the
122 evidence for selective sweeps of virus-resistance genes in infected replicates.

123 Only 6 mutations showed a frequency close to 100% (Supplementary Table 1) in all the infected
124 replicates. Of these 6 mutations, 3 involved non-synonymous changes, affecting an ATP-
125 dependent helicase/deoxyribonuclease, an orotate phosphoribosyltransferase and a
126 sodium/glucose cotransporter. The first two are related to helicase/exonuclease activities and to
127 the synthesis of pyrimidines, respectively, so they did not seem to have a direct relationship with
128 virus resistance. The third mutation, affecting the stop codon in the synthesis of the sodium/glucose
129 cotransporter, could be involved in the resistance, as it affects a transmembrane protein. However,
130 upon further examination, we found that both resistant and sensitive cells had the same mutation,
131 confirming that it was unrelated to resistance. In addition, it was subsequently found that cells that
132 regained susceptibility to the virus retained all the mutations mentioned above (see below and
133 *Mutations Supplementary Information* for further details). Therefore, no mutations could be
134 unequivocally tied to the observed population recovery phenomenon in the infected cultures.

135 According to previous studies (30), these dynamics after viral infection could be explained by the
136 integration of the viral genome into the chromosome of its host, yielding lysogens resistant to
137 superinfection with the same virus. Although EM1 lacked any lysogeny-associated traits in its
138 genome, including excisionase and integrases (Supplementary Table 2), the reads of the infected
139 C_F cultures were reexamined to search for hybrid host-virus reads, which would signify integration
140 into the chromosome (see Methods). No hybrid reads were found, and therefore recovery cannot
141 be attributed to virus integration. However, we observed a remarkably high sequencing depth of
142 the virus genome within infected C_F cultures, averaging 146 nt/position, while the cellular
143 chromosome exhibited 116 nt/position (Supplementary Table 3). This similar level of sequencing

144 depths suggests that viral genomes are maintained intracellularly in the recovered cultures, albeit
145 not via integration as a prophage.

146 **Infected cells with episomally maintained viruses comprise part of the recovered *Sal. ruber***
147 **population**

148 The lack of evidence for mutations related to virus resistance or integrated prophage within
149 recovered *Sal. ruber* populations led us to hypothesize that recovered bacterial populations
150 infected by viruses might maintain viral genomes intracellularly in an episomal form. To explore
151 this alternative, we grew colonies from time point C_0 (initial *Sal. ruber* M1) and C_F (final recovered
152 cells). Twenty individual colonies from both C_0 and C_F were grown in liquid medium and PCR-
153 tested for the presence of the EM1 virus. As expected, all C_0 colonies tested positive with the
154 specific primers for *Sal. ruber* M1 but tested negative for the virus. However, all the final colonies
155 from the infected cultures tested positive for the EM1 virus. Three randomly selected cultures from
156 the C_F, colonies that tested PCR positive for the virus (which we refer to as 1R, 2R and 3R
157 respectively), were stained with SYBR^{TM}Gold and observed under the epifluorescence microscope
158 (Fig. 2a). After observation of more than thirty fields per culture, extracellular virions were not
159 observed in any case. Hence, although EM1 virus was present in the culture, its virions were not
160 detected extracellularly. The intracellular presence of viral genomes was confirmed by pulsed field
161 gel electrophoresis (PFGE) with DNA from the final colony 1R, but not from the control C_0 colony
162 (wild type *Sal. ruber* M1). The PFGE showed a band with the size of the EM1 virus genome (35
163 kb) in 1R, which was confirmed by Southern blot hybridization with an EM1-specific probe (Fig.
164 2b). These results, in conjunction with the sequencing data that revealed no signs of integration
165 (no hybrid host-virus reads were found), the lack of integrases and/or recombinases in the genome
166 of EM1 (Supplementary Table 2), supports the hypothesis that the EM1 virus was maintained in
167 an episomal form within *Sal. ruber* M1 recovered populations. In addition, the terminal
168 redundancy found in sequencing may indicate that it is maintained within cells as a circular
169 episome.

170 **Episomal maintenance of viruses protects recovered cells from subsequent infection and**
171 **viral-induced lysis**

172 To test whether the acquisition and episomal maintenance of the virus had an influence on the
173 recovered cell growth, we conducted growth experiments on 1R and compared the population
174 dynamics to that of the wild type *Sal. ruber* M1 (Fig. 3a). We found no statistical differences in
175 the reached OD or growth dynamics between 1R and *Sal. ruber* M1 (*Modeling Supplementary*
176 *Information: Sal. ruber M1 wild-type and 1R (pseudolysogen) growth comparison*). Hence, there
177 is no evidence that viral acquisition provides a direct cost or benefit to host growth. However, the
178 benefits of intracellular maintenance of viral genomes may be contextual.

179 During typical lysogeny, the prophages can protect hosts from viral infection and lysis via
180 superinfection exclusion (31, 32, 33). We hypothesize that similar principles may apply to
181 recovered bacterial populations. To test for superinfection exclusion in recovered populations, we
182 conducted spot test assays with 1R and the wild type *Sal. ruber* M1. In both cases, we plated cells
183 and then overlaid agar plates with spots of EM1 virus serially diluted from 10^{10} PFU/ml to 10^{4}
184 PFU/ml (see Methods). The wild type strain was susceptible to EM1 infection, whereas 1R
185 exhibited resistance (Fig. 3b). We interpret the results of the spot assay experiment to imply that
186 episomal maintenance of the EM1 virus confers protection against subsequent EM1 infection and
187 lysis. Furthermore, by conducting an adsorption assay with 1R and the wild type *Sal. ruber* M1,
188 we found that protection against subsequent EM1 infection occurs at the surface level, i.e.,
189 preventing effective adsorption (Extended Data Fig. 2).

190 Finally, to test how stable is the intracellular maintenance of EM1, we plated the 1R strain and
191 picked colonies at random to test for the presence of the virus by PCR. The results showed that 13
192 of 17 colonies retained the virus (*Mutations Supplementary Information*). A spot test with EM1 on
193 the cultures derived from the 17 colonies revealed that only those strains that had lost the virus
194 genome were sensitive to EM1 infection, confirming that the resistance was due to the virus
195 acquisition and episomal maintenance. Subsequent genomic sequencing of 3 of these sensitive and
196 3 resistant colonies (all derived from 1R) showed that the mutations observed in recovered cultures
197 following the infection (see above) had not been lost and therefore were not involved in the
198 development of resistance to EM1 infection (*Mutations Supplementary Information*). The
199 reappearance of sensitive strains within the 1R recovered population suggests that the viral genome
200 is not replicating synchronously or faithfully segregated with the host chromosome. Consistently,
201 no marker was found in the virus genome that would indicate cell-synchronous replication and

partition, such as the Par system of bacteriophage P1 (34) (Supplementary Table 2). Therefore, we hypothesize the viral persistence inside recovered cells is enabled through asymmetric episomal virus transmission during cell division consistent with a pseudolysogenic state (see (24)). For the remainder of the manuscript, we refer to bacterial populations post-infection as 'recovered' and use the term resistant pseudolysogens to refer to the subset of bacterial populations that have episomally maintained the virus genome and are resistant to subsequent infection and lysis by the same virus.

Bacterial population recovery depends non-monotonically on MOI

The spot assay experiment yielded a counter-intuitive result. When high virus concentrations were added on the plates of wild type *Sal. ruber* M1 at levels between MOI of 10-100, we observed growth of cells in the center of spots. This suggests that there may be a MOI dependence to the initiation of pseudolysogeny, akin to that found in classic studies of lysogeny in which the probability of lysogeny increases with increasing MOI (21, 35, 36). Hence, cultures with cells infected by multiple viruses may be more likely to yield pseudolysogens which can grow even in the presence of viruses. To explore the MOI-dependence of recovery further, *Sal. ruber* M1 was infected with EM1 at MOIs ranging from 0.01 to 10 viruses per host cell. The M1 population was infected during its exponential growth phase (66 h). The population dynamics (Fig. 3c) exhibit dip and recovery dynamics for MOI 1, 5 and 10 in a similar fashion to the initial infection curve experiment. In contrast, population dynamics for MOI 0.01 and 0.1 solely exhibit growth, albeit slightly slower than in the control population. Notably, the final cell densities in the experiments with MOI 1, 5 and 10 were non-monotonically related to MOI, i.e., the OD values were 0.22 +/- 0.01, 0.18 +/- 0.02 and 0.27 +/- 0.01 for MOI 1, 5, and 10, respectively. The OD value at time 230 hours for MOI 10 was statistically significantly different from the OD value for MOI 1 (t-test, $p=0.041$) and MOI 5 (t-test, $p=0.038$). Note that we could not reject the null hypothesis that the OD values at time 230 hours for MOI 1 vs 5 were statistically different (t-test, $p=0.206$). These results raise the question: if EM1 generates resistant pseudolysogens (as was confirmed in the spot assay experiment for 1R (see Fig. 3b)), then why would recovery dynamics depend non-monotonically on MOI?

230 Typically, superinfection exclusion requires certain cellular rearrangement post-infection (31, 32,
231 37). As such, we hypothesize that multiple EM1 viruses can jointly infect the same *Sal. ruber* M1
232 cell, insofar as multiple infections precede the development of resistance (38). For example, given
233 a MOI of 10 and assuming that all virions have adsorbed to the cell and injected their genomes,
234 the infection would yield an average of 10 viruses per cell with a standard deviation of ~3.
235 Therefore, to test whether superinfection was possible in this system, we performed adsorption
236 assays with the wild type *Sal. ruber* M1 and EM1 at MOI of 0.01 and 10 (Fig. 3d). In the case of
237 MOI 0.01, the decrease of free viruses was equivalent to that expected in theory for complete
238 adsorption of virions onto cells (i.e., approximately 1% of cells should be infected). In the case of
239 MOI 10, the exponential decrease of free viruses plateaus at ~20%, implying that 80% of virions
240 adsorbed to cells, consistent both with superinfection (i.e., the average cellular-level MOI would
241 be 8) and interference that limits viral superinfection at high MOI. Hence, we conclude that
242 superinfection of *Sal. ruber* M1 is possible by the EM1 virus given sufficiently short intervals
243 between infection events even if the development of a superinfection exclusion state prevents
244 subsequent infection over the long term in resistant pseudolysogens.

245 **Scaling-up the dynamical effects of pseudolysogeny from cells to populations**

246 The contextual impact of superinfection raises questions on how pseudolysogeny modulates
247 recovery dynamics, in light of three key empirical observations (Fig. 3c). First, the *Sal. ruber* M1
248 populations infected at MOI 0.1 and 0.01 do not exhibit an observable population decline. Second,
249 the M1 host population recovers to a higher population densities when infected at MOI 10
250 compared to MOI 5 and MOI 1, highlighting a non-monotonic relationship between viral levels
251 and population-level lysis. Third, when infected at MOI 10, the *Sal. ruber* M1 population does not
252 crash immediately upon infection and maintains persistent transient growth post infection. To
253 connect mechanisms occurring at cellular-scales with these population-level dynamics, we
254 developed a nonlinear ordinary differential equation (ODE) model of the EM1 virus interacting
255 with *Sal. ruber* M1 hosts (Fig. 4). The model includes dynamics of resources (R), sensitive cells
256 (S), pseudolysogens (P) and virus particles (V) (39). We separate pseudolysogens into "early" (P_e)
257 and "fully developed" pseudolysogens (P_f), where viruses can infect sensitive cells and early
258 pseudolysogens (consistent with findings of Fig. 3d) which then transition to become resistant, P_f
259 types (consistent with findings of Fig. 3b). We account for cellular-level multiplicity of infection

of the pseudolysogens through a superscript $^{[k]}$ where k denotes the number of viral genomes per cell e.g., $P_e^{[2]}$ denotes the number of early pseudolysogens with 2 viral genome copies. The number of viruses able to infect a single cell is limited, consistent with adsorption results from Fig. 3d (details in Extended Data Fig. 3). Cell division for both sensitive cells and pseudolysogens is modeled as a function of resource consumption. Full details of the model specification and parameters are provided in the Supplement (*Modeling Supplementary Information: Main Model).*

Simulated population dynamics (Fig. 5a) recapitulate the key empirical observations (as shown in Fig. 3c). The match between theory and experiment is driven by the following mechanisms. First, the model assumes that host lysis decreases with decreasing resources (40, 41). In Fig. 5b, we show that decoupling host lysis from resource concentrations leads to a rapid crash in *Sal. ruber* dynamics amongst the low MOI populations that is inconsistent with experimental observations. Second, the model assumes that cellular lysis rates decrease as a function of increasing cellular MOI (42, 43). In Fig. 5c, we show that if lysis rates are independent of cellular MOI, then population crashes are most apparent at the highest MOI and decrease with decreasing MOI, inconsistent with experimental observations. Third, we assume that pseudolysogens divide and that their daughter cells can inherit viral genomes, albeit randomly, from the parent cell (akin to random segregation of episomal elements (44)). In Fig. 5d, we show that if pseudolysogens do not divide then the *Sal. ruber* population at MOI 10 (yellow curve) immediately dips upon infection at 66 hours (blue dotted line) and there is no persistent transient growth, thereby inconsistent with the experimental dynamics. In *Modeling Supplementary Information*: *Subsets of main model with corresponding dynamics,* we explore all potential combinations of the presence/absence of each mechanism and find that the model only recapitulates observed dynamics when all three mechanisms operate jointly. Hence, we contend that each of these elements (resource-dependent lysis, latent period delays in multiply infected cells, and pseudolysogen cellular division) are necessary to explain experimentally observed dynamics of the EM1 virus and its host across 3 orders of magnitude difference in initial ratios of virus to host. The details of how all the model features are implemented is highlighted under *Modeling Supplementary Information: Key Model Features* and *Modeling Supplementary Information: Viral passage in superinfected pseudolysogens*. Finally, we note that the results are robust to variation in the variability associated with the passage of episomally maintained viruses to daughter cells during replication (*Modeling Supplementary Information: Episomal viral replication*).

291 **Episomal maintenance of viruses and the population-scale maintenance of virus-microbe**
292 **coexistence**

293 Finally, we set out to explore the extent to which episomal maintenance of viruses inside recovered
294 bacterial populations could enable virus-microbe coexistence over longer time scales. The
295 persistence of the virus within the pseudolysogen population was tested by transferring
296 pseudolysogen 1R every 9-10 generations to fresh medium. We made four such transfers, resulting
297 in ~ 40 generations of pseudolysogen growth and cell division (Extended Data Fig. 4a). At the end
298 of the exponential phase of each transfer, we conducted a PCR test and found that the virus was
299 not lost over time (Extended Data Fig. 4b). Upon qPCR analysis, we found that the ratio of virus
300 genome/chromosome was close to 1 in the first transfer and upon further transfers, the ratio
301 increased to 2-3 virus genomes per chromosome of M1 and was maintained at this level (Extended
302 Data Fig. 4c). To determine whether viral resistance was maintained within the population, cells
303 from each of the aforementioned transfers were exposed to EM1 through a spot test. We found
304 that the cells from every transfer exhibited resistance to additional infection (Extended Data Fig.
305 5). Next, to observe how the pseudolysogens might ecologically interact with other *Sal. ruber*
306 strains, we conducted spot tests in which eight strains of *Sal. ruber* used routinely in our laboratory
307 were individually exposed to pseudolysogen 1R. We observed that *Sal. ruber* M1, the only strain
308 sensitive to the EM1 virus, was killed while the rest of the seven strains were maintained (Extended
309 Data Fig. 6). Similar dynamics have been observed with temperate viruses, where lysogens induce
310 and release free virions as a weapon to kill sensitive cells in shared environments (45). We
311 hypothesize that a subset of pseudolysogens of *Sal. ruber* reactivate the lytic pathway, releasing
312 virions that infect sensitive competitors, generating a mix of pseudolysogens and increasing the
313 level of extracellular virions.

314

315 **DISCUSSION**

316 Here we explored the dynamics arising from interactions between a virulent virus (EM1) and one
317 strain of a prevalent and globally dispersed bacterial host found in hypersaline environments (*Sal.*
318 *ruber* M1). We found that *Sal. ruber* M1 populations reproducibly recover from infections by EM1
319 viruses across three orders of magnitude variation in MOI. Notably, M1 bacterial populations

320 recover to higher densities when infected with more viruses (MOI=10) than with less viruses (MOI
321 1 or 5) while recovering to densities comparable to those of non-infected controls for MOI levels
322 of 0.1 or 0.01. Both sequence and experimental evidence suggest that recovered populations have
323 a significant fraction of cells with episomally maintained virus genomes that pass asymmetrically
324 from mother to daughter cells in the absence of synchronized replication with their cellular hosts.
325 Subsequent infection experiments revealed that these cells with episomally maintained virus
326 genomes (i.e., pseudolysogens) are resistant to infection and lysis by the original virus, providing
327 an opportunity to explore mechanisms by which infection recovery could stabilize bacteria-virus
328 feedback. We developed and analyzed a nonlinear population dynamics model that recapitulated
329 key features of the MOI dependent recovery dynamics that depend on the potential joint infections
330 of cells, lysis inhibition via superinfection immunity, and lysis inhibition due to resource
331 limitation. Altogether, the initiation and maintenance of pseudolysogeny stabilizes short-term
332 population dynamics while providing a mechanism for long-term coexistence of viruses and their
333 bacterial hosts in extreme environments.

334 The current study connects cellular-level interactions to feedback mechanisms that stabilize virus-
335 host population dynamics that could otherwise lead to population collapse, especially at high MOI
336 values. While previous studies have shown similar recovery dynamics in different virus-host
337 systems (46, 47, 48, 49), there has been limited effort to explain the mechanisms responsible.
338 Studies observing recovery dynamics phenomenon with temperate viruses have pointed to
339 emergence of resistant lysogens which are protected against further infections (28, 30). However,
340 bacterial population recovery has also been observed in viruses without any lysogeny markers as
341 well (50, 51), in which the emergence of resistance has been overlooked or simply attributed to
342 spontaneous mutations of the host (52, 53). Here, recovery dynamics could not be attributed to
343 lysogeny given the use of the *Sal. ruber* M1-EM1 system where EM1 is strictly virulent. The
344 recovery dynamics observed here was also highly reproducible, inconsistent with recovery due to
345 the emergence and expansion of spontaneous resistant mutants that grow from low to high
346 frequency where substantial variability is a hallmark feature of dynamics (29). Furthermore, our
347 analysis revealed no clear resistance-associated mutations in the recovered M1 populations.
348 Similarly, we also identified lysis inhibition at high MOI and/or when resources are limited as an
349 essential part of explaining the MOI-dependence of recovery dynamics. Lysis inhibition has
350 commonly been noted in infection of *Escherichia coli* by T4 (40, 42, 53, 54), with some studies

351 suggesting that it plays a key role in the maintenance and development of *E. coli*-T4
352 pseudolysogens (24, 54). We hypothesize that lysis inhibition could similarly be a key feature of
353 pseudolysogeny in the *Sal. ruber* M1-EM1 system, allowing for persistent infection in starved
354 conditions and/or under high MOI.

355 Our combined study comes with caveats. First, we focused primarily on contextual benefits of
356 pseudolysogeny, noting that identifying direct impacts of episomal maintenance of viruses on
357 cellular fitness has limited support (55). While we found that there were no statistical differences
358 between the growth rate of pseudolysogens and wild type host cells, we found that pseudolysogeny
359 provided surface-level protection against further infection. Furthermore, we found that loss of
360 episomally maintained viruses renders pseudolysogens sensitive to further infection. Hence, viral
361 acquisition comes with a cost (the risk of lytic infection) but is key to enabling surface-level
362 resistance and population level recovery. More work is needed to understand when pseudolysogens
363 become resistant and the cellular mechanisms underlying transient protection to infection. We also
364 found that *Sal. ruber* strains that were sensitive to the EM1 virus were killed in the presence of
365 pseudolysogens. Similar dynamics have been observed with temperate viruses of *Roseobacter*,
366 where lysogens induce and release virions to kill competing sensitive strains in head-to-head
367 experiments (45). We hypothesize that *Sal. ruber* M1 pseudolysogens may switch from a
368 maintenance to an actively infected state, e.g., when episomal numbers are low and/or when
369 resources become available. Again, future work will be needed to elucidate the cellular drivers of
370 lytic initiation and the extent to which intrinsic or extrinsic heterogeneity plays a role in the lysis
371 of pseudolysogens that release EM1 viruses that may then infect and kill competing sensitive
372 strains and potentially initiate new pseudolysogens.

373 In closing, this study reveals how feedback mechanisms at the cellular scale can transform
374 population dynamics leading to non-monotonic relationships between virus infection pressure and
375 bacterial impacts. Put simply: for strictly lytic viruses, more infection does not always result in
376 more killing. Within the *Sal. ruber* M1-EM1 bacteria-virus model system, we have identified
377 feedback mechanisms that limit lysis, whether because of multiple infections, resource limitation,
378 or the establishment of an episomally maintained virus (i.e., a pseudolysogen). Each of these
379 mechanisms stabilizes virus-microbe population dynamics. We recognize that it is challenging to
380 move from experimental settings to extreme field conditions, hence we are forced - for now - to

381 speculate that pseudolysogeny may be an evolutionarily adaptive strategy for obligately lytic
382 viruses to preserve hosts until environmental conditions improve or host density increases (23, 24,
383 56). Depending on the durability of viruses extracellularly, such a balance between infection and
384 production may help to explain virus:host ratios ranging from 10 to as high as 300 in the face of
385 fluctuating conditions (14). More broadly, it may be of some value to explore other, related cellular
386 mechanisms that stabilize virus-host population dynamics, enabling reproducible recovery
387 dynamics seen in ecosystems outside hypersaline environments, such as the bloom-bust dynamics
388 observed in oceanic *Emiliania huxleyi* populations after infection by EHV at high MOI (46, 57) or
389 the long-term persistence of crAss-like phage crAss001 and its host (58). Overall, the results from
390 this work highlight the ecological relevance of exploring a continuum of viral infection strategies
391 beyond the dichotomous options of lysis or lysogeny.

392

393 **METHODS**

394 **Growth conditions and DNA extraction**

395 *Sal. ruber* strain M1 was grown aerobically with gentle shaking (60 rpm) at 37 ºC in 25% SW (sea
396 water) with 0.2% yeast extract (59). *Sal. ruber* M1 was infected with the lytic virus EM1 (27),
397 using a multiplicity of infection (MOI) of 0.01 plaque forming units (PFUs) per cell at time 0 h.
398 Briefly, viruses were mixed with cells at exponential phase (optical density, OD, at 600 nm=0.3)
399 and incubated during 30 minutes at room temperature without shaking to facilitate the adsorption.
400 After the adsorption, the abovementioned culture medium was added up to 25 ml and incubated
401 as previously described. Infections were monitored by OD at 600 nm. Non-infected *Sal. ruber* M1
402 was grown as the control. All experiments were conducted in triplicate. Another curve was made
403 with the same methodology but using a MOI of 0.1 and 10 replicates in both control and infection.

404 Bacterial pellets of the initial (C_0, before virus addition) and final cells (C_F) of the curves performed
405 using a MOI of 0.01 were obtained by centrifugation at 17.000 xg during 10 min. The cells were
406 washed three times with sterile medium, the supernatant removed and the cell pellets stored at -80
407 ºC. C_0 and C_F DNAs were extracted with the DNeasy Blood & Tissue Kit (Qiagen, Hilden,

408 Germany) following the manufacturer's protocol, and nucleic acids eluted in 70 µl of milli-Q water
409 and quantified using Qubit 2.0 Fluorometer (Life Technologies, Carlsbad, USA).

410 **DNA sequencing and bioinformatic analysis**

411 DNA was sequenced on an Illumina HiSeq (2 x 150 bp) at Novogene (Novogene, Seur, UK).
412 Primers and adapters were removed from sequences, and reads were filtered based on quality
413 scores using Trimmomatic v0.36.0 (60). Trimmed reads were assembled using SPAdes v3.13.1
414 with the trusted option using the reference genome of *Sal. ruber* M1 as scaffold (61). The mean
415 sequencing depth was calculated by a BLASTN-recruitment analysis where the assembled contigs
416 were used as reference.

417 For the search for hybrid host-virus reads, a BLASTN of the trimmed reads was performed, using
418 the genome of *Sal. suber* M1 of NCBI as a database (GenBank accession number:
419 NZ_CP030364.1). The reads with >95% ID were filtered by best hit and extracted. No horizontal
420 coverage filter was used. Another BLASTN analysis was performed with these reads using the
421 genome of the EM1 virus of NCBI as a database (GenBank accession number: NC_042348.1) with
422 the same parameters. No hybrid host-virus reads were found.

423 Mutations generated during the infective process were identified comparing reads from C_F with
424 the reference contigs assembled from C_0 using Geneious software 6.1.8 (Biomatters, Auckland,
425 New Zealand) with a minimum variant frequency of 0.01% and a coverage >25% to the mean
426 coverage.

427 **PCR and epifluorescence microscopy**

428 Cells from C_0 and C_F were diluted and plated on SW 25% with 0.2% yeast extract agar plates
429 (concentration 2%) and incubated at 37 °C for 30-45 days until colonies visualization. Twenty
430 colonies from every point (C_0 and C_F) were grown in 2 ml of culture medium at 37 °C and 60 rpm.
431 Once the cultures grew to late exponential phase, 200 µl of each were washed three times by
432 centrifugation (see above). DNA was extracted from washed pellets by boiling at 100 ºC for 10
433 min after resuspending the cells in 80 µl of milli-Q water. Two parallel PCR reactions were
434 performed with each DNA, using specific primers for *Sal. ruber* M1 and the virus EM1
435 (Supplementary Table 4). PCR reactions were carried out in a final volume of 25 µl, containing:

436 0.75 µl of 1.5 mM $MgCl_2$, 2.5 µl of 10X reaction buffer, 0.5 µl of 10 mM dNTPs, 0.1 µl of Taq
437 polymerase (5 U/µl, Invitrogen, Waltham, USA), 0.5 µl of 10 µM primers, 1 µl of extracted DNA
438 and milli-Q water to complete the final volume. PCR conditions are described in Supplementary
439 Table 5. PCR products were electrophoresed and UV-visualized after staining with ethidium
440 bromide (100 µg/ml).

441 Three random cultures from C_F colonies that were PCR positive for both *Sal. ruber* M1 and the
442 EM1 virus (named 1R, 2R and 3R) were selected for the visualization of extracellular virions by
443 SYBR^{TM}Gold staining (62). Briefly, 100 µl of the culture were fixed with formaldehyde (4% final
444 concentration) for 1 h at 4 ºC. Fixation was stopped by adding phosphate-buffered saline (PBS)
445 1X up to 1 ml. Twenty microliters (equivalent to 2 µl of sample) were filtered through 0.02 µm
446 Anodisc 25 filters (Whatman Int. Ltd, Maidstone, UK) to retain cells and viruses. Filters were
447 stained with SYBR^{TM}Gold (25X) for 15 min, washed twice for 1 min with milli-Q water and
448 visualized with an epifluorescence microscope (Leica, type DM4000B).

449 **Pulsed-field gel electrophoresis (PFGE) and Southern Blot**

450 One ml of liquid cultures of C_0, PCR positive for M1, and C_F, PCR positive for M1 and EM1, were
451 centrifuged and the cell pellets mixed with agarose at 0.8% (final concentration) to obtain plugs,
452 as detailed in Santos et al., 2007 (63). Plugs were incubated overnight at 50 ºC in ESP (0.5 M
453 EDTA, pH 9.0, 1% N-laurylsarcosine, 1 mg ml^{-1} proteinase K) for cell lysis and virion
454 disruption and stored at 4 ºC. DNA was separated by PFGE on a 1% LE agarose gel in 0.5X TBE
455 buffer, using a Bio-Rad CHEF DR-III System (Bio-Rad, Richmond, USA), under the following
456 conditions: 8–12 s pulse ramp, 6 V/cm, at 14 °C for 30 hrs. After electrophoresis, gels were stained
457 with ethidium bromide (100 µg/ml) for 10 min, washed with distilled water for 30 min, and UV-
458 visualized with a transilluminator.

459 Agarose gels were transferred to a positively charged nylon membrane (GE Healthcare,
460 Buckinghamshire, UK) as previously described (64). In parallel, DNA from the EM1 virus was
461 labelled to be hybridized against the membrane using the DIG High Prime DNA Labelling and
462 Detection Starter Kit II (Roche, Mannheim, Germany), following manufacturer's instructions.

463 **Growth curves, spot tests and adsorption assays**

464 *Sal. ruber* M1 wild type (as a control) and pseudolysogen 1R were grown in liquid, transferred to
465 fresh media (1% v/v) and incubated at 37 ºC with gentle shaking at 60 rpm. Cellular density was
466 measured by OD at 600 nm. The growth curves of *Sal. ruber* M1 wild type and pseudolysogen 1R
467 were compared for statistical differences using 99% confidence intervals obtained through the
468 Delta method (*Modeling Supplementary Information: Sal. ruber M1 wild-type and 1R*
469 *(pseudolysogen) growth comparison*).

470 To test the resistance/susceptibility of *Sal. ruber* M1 wild type and pseudolysogen 1R to the EM1
471 virus, both hosts were exposed to the virus by a spot test. Four ml of molten 0.7% top agar of 25%
472 SW with 0.2% yeast extract were mixed with 500 µl of bacterial cultures at exponential phase and
473 plated on solid medium. Once solidified, 3 µl of the EM1 virus, tittered at 10^{10} PFUs/ml and diluted
474 10^2, 10^4 and 10^6 times, were added to the lawn. The spotted plates were left to dry and incubated
475 at 37 ºC for 10 days. The detection of a clearance zone was interpreted as evidence of viral lysis
476 while the areas exhibiting growth were attributed to resistance against EM1.

477 An adsorption assay was performed with the EM1 virus and *Sal. ruber* M1 wild type. Cultures in
478 exponential phase were diluted with fresh medium to an optical density of 0.3 and $2x10^8$ cells were
479 mixed with $2x10^6$ PFU (MOI=0.01) or $2x10^9$ PFU (MOI=10) of the EM1 virus. This was
480 considered as the initial time. It was incubated at 37 ºC and 60 rpm. Aliquots of 150 µl were taken
481 along 2 h (at 15, 30, 45, 60, 90 and 120 min), centrifuged at 17.000 xg for 8 min, and 120 µl of the
482 cells-free supernatant were stored in ice. The number of infective free viruses was measured by
483 plaque assay, diluting the supernatants in sterile SW 25% and mixing 100 µl of each with 500 µl
484 of *Sal. ruber* M1 wild type in exponential phase. Four ml of top agar were added and this was
485 plated on solid plaques. After solidifying, the plates were incubated at 37 ºC for 10 days until
486 plaques were visible. The number of free infective viruses (PFU/ml) were counted and represented.
487 A control of the viral decay of the EM1 virus was added, in which the virus was incubated without
488 host. All the experiments were conducted in triplicate.

489 To get more information about the resistance mechanism, an adsorption assay was performed with
490 the EM1 virus and *Sal. ruber* M1 wild type and pseudolysogen 1R with a MOI of 0.01 as described
491 above.

492 To calculate the adsorption rate, the graph of the free infective viruses (PFU/mL) was plotted with
493 respect to time and fit to an exponential function. As the assay was conducted within a 120 min
494 time period and the latent period of the EM1 virus is around 21-22 h, we can assume that there is
495 negligible killing and the susceptible host population stays constant at $S = 2\text{x}10^8$ cells. We fit the
496 adsorption data to the function $V = V_0\, e^{-\phi S t}$ and get an adsorption rate $\phi \approx 4\text{x}10^{-10}$ ml/h (Fig.
497 S10).

498 **Infection curves at varying MOIs and revival of lysis in pseudolysogens**

499 *Sal. ruber* M1 wild type was grown at 37 ºC and 60 rpm. The EM1 virus was added at 67 h at
500 middle exponential phase. Cultures were infected with a MOI of 0.01, 0.1, 1, 5 and 10 plaque
501 forming units (PFUs) per cell in separate experiments. Infections were monitored by OD at 600
502 nm. *Sal. ruber* M1 was grown without viruses as a control. All experiments were conducted in
503 triplicate.

504 A total of $2\text{x}10^8$ cells from the end of each infection curve were transferred to 4 ml of fresh medium
505 (SW 25% with 0.2% yeast extract). This caused all cultures to be diluted to an OD of
506 approximately 0.1. Cultures were monitored by OD at 600 nm.

507 **Numerical Simulations**

508 All the numerical simulations were performed on Python 3.11.5 through the Jupyter IDE. To solve
509 the model ODEs and obtain the simulated results, we used the numerical integration module *odeint*
510 from the *SciPy* package. To convert the experimental OD measurements to concentrations, we fit
511 a calibration curve using the *curve_fit* module from the *SciPy* package. All the code that can
512 reproduce the simulated results seen in this paper are available on the Github:
513 https://github.com/aranilah/SalruberM1_EM1_recovery/tree/main

514 **Transfers of pseudolysogen 1R to fresh media, PCR and qPCR**

515 In order to assess if the EM1 virus was with generations, pseudolysogen 1R was transferred four
516 times to fresh media. Briefly, pseudolysogen 1R was transferred in triplicates to fresh media (1 %
517 v/v) and incubated at 37 ºC with shaking at 60 rpm, measuring the growth by OD at 600 nm. At
518 the late exponential phase cultures were transferred again to fresh media until a total of 4 transfers.

519 A spot test of each transfer was also carried out as previously mentioned to check if the different
520 transfers of pseudolysogen 1R were still resistant to the virus. Moreover, 100 µl of each transfer
521 were fixed with formaldehyde (0.5% final concentration to avoid PCR inhibition) for 1 h at 4 ºC.
522 Fixation was stopped by adding phosphate-buffered saline (PBS) 1X up to 1 ml.

523 To eliminate free viruses, assuming that viruses could have been spontaneously released during
524 the transfer periods, the fixed samples were centrifuged at 17.000 xg during 10 min and washed
525 with PBS five times. PCR reactions for *Sal. ruber* M1 and the EM1 virus were carried out as
526 mentioned above, with 1 µl of the fixed and washed cells as DNA template (first, we checked that
527 the PCR initial thermal shock was sufficient for cell lysis; data not shown).

528 Once the presence of EM1 was detected in all the transfers, a qPCR was performed to monitor
529 virus concentration along the subsequent transfers. The qPCR assay was conducted using TaqMan
530 hydrolysis probes (Supplementary Table 4) labeled with hexachlorofluorescein (for *Sal. ruber* M1)
531 and fluorescein (for EM1). The experiment was carried out using the standard run in a
532 StepOnePlus™ PCR System (Life Technologies, Carlsbad, USA) in a 10 µl reaction mixture with
533 PrimeTime™ Gene Expression Master Mix (Integrated DNA Technologies, Coralville, USA). The
534 reaction contained: 5 µl of 2X Master Mix, 0.2 µl of each 10 µM primer, 0.2 µl of 10 µM TaqMan
535 probe, 1 µl of fixed sample and milli-Q water to complete volume. Conditions are detailed in
536 Supplementary Table 6. The results were analyzed with the Applied Biosystems StepOne™
537 Instrument program. All samples were run in triplicate (including the standards and negative
538 controls).

539 **Plating of pseudolysogen 1R, mutation screening and spot test**

540 Pseudolysogen 1R at late exponential phase was plated on solid medium (SW 25% with 0.2%
541 yeast extract and 2% agar) to obtain individual colonies. After two months of incubation, 50
542 colonies developed, which were picked and transferred to 1 ml of liquid media each. The presence
543 of the EM1 virus and the resistance/susceptibility was checked by PCR and spot test as previously
544 described.

545 To check if the colonies had the mutation affecting the sodium/glucose cotransporter, primers were
546 designed to amplify the specific region (Supplementary Table 7). DNAs of the 6 selected colonies

547 picked in 1 ml of medium and *Sal. ruber* M1 wild type (as a control of the mutation) were extracted
548 by boiling as previously described and PCR reactions done as described previously. PCR
549 conditions are described in Supplementary Table 8. PCR products were visualized under
550 ultraviolet light after staining with ethidium bromide (100 µg/ml). Products were sequenced with
551 Sanger method at Stab Vida (Stab Vida, Caparica, Portugal) and analyzed with Geneious software
552 6.1.8 (Biomatters, Auckland, New Zealand).

553 Eight strains of *Sal. ruber* (M1, M8, M31, P13, P18, SP38, SP73 and RM158) were exposed to
554 pseudolysogen 1R through spot test as previously described, adding spots of 3 µl of 1R at late
555 exponential phase and diluted 10^2, 10^4 and 10^6 times on the double layer formed by the strains.

556 **One step growth curve**

557 Burst size was determined after carrying out a one-step growth experiment as detailed in
558 Kropinski, 2018 (65) (Supplementary Table 9).

559

560

561

562

563

564

565

566

567

568

569

570 **REFERENCES**

571 1. Shiklomanov, I. A. World water resources: a new appraisal and assessment for the 21st
572 century (UNESCO-IHP, 1998).

573 2. Mutlu, M. B. et al. Prokaryotic diversity in Tuz Lake, a hypersaline environment in Inland
574 Turkey. FEMS Microbiol. Ecol. 65, 474–483 (2008).

575 3. Ramos-Barbero, M. D. et al. Prokaryotic and viral community structure in the singular
576 chaotropic salt lake Salar de Uyuni. Environ. Microbiol. 21, 2029–2042 (2019).

577 4. Boujelben, I. et al. Virioplankton Community Structure in Tunisian Solar Salterns. Appl.
578 Environ. Microbiol. 78, 7429–7437 (2012).

579 5. Ventosa, A. *Unusual micro-organisms from unusual habitats: hypersaline environments*
580 (Cambridge University Press, 2006).

581 6. Gomariz, M. *et al.* From community approaches to single-cell genomics: the discovery of
582 ubiquitous hyperhalophilic Bacteroidetes generalists. *ISME J.* 9, 16–31 (2015).

583 7. Antón, J. *et al. Salinibacter ruber* gen. nov., sp. nov., a novel, extremely halophilic member
584 of the Bacteria from saltern crystallizer ponds. *Int. J. Syst. Evol. Microbiol.* 52, 485–491 (2002).

585 8. Viver, T. *et al.* Diversity of extremely halophilic cultivable prokaryotes in Mediterranean,
586 Atlantic and Pacific solar salterns: Evidence that unexplored sites constitute sources of cultivable
587 novelty. *Syst. Appl. Microbiol.* 38, 266–275 (2015).

588 9. Mora-Ruiz, M. del R. *et al.* Biogeographical patterns of bacterial and archaeal communities
589 from distant hypersaline environments. *Syst. Appl. Microbiol.* 41, 139–150 (2018).

590 10. Viver, T. *et al.* Description of two cultivated and two uncultivated new *Salinibacter*
591 species, one named following the rules of the bacteriological code: *Salinibacter grassmerensis* sp.
592 nov.; and three named following the rules of the SeqCode: *Salinibacter pepae* sp. nov.,
593 *Salinibacter abyssi* sp. nov., and *Salinibacter pampae* sp. nov. *Syst. Appl. Microbiol.* 46, 126416
594 (2023).

595 11. Santos, F. *et al.* Culture-Independent Approaches for Studying Viruses from Hypersaline
596 Environments. *Appl. Environ. Microbiol.* 78, 1635–1643 (2012).

597 12. Wigington, C. H. *et al.* Re-examination of the relationship between marine virus and
598 microbial cell abundances. *Nat. Microbiol.* 1, 1–9 (2016).

599 13. López-García, P. *et al.* Metagenome-derived virus-microbe ratios across ecosystems. *ISME*
600 *J.* 17, 1552–1563 (2023).

601 14. Di Meglio, L. *et al.* Seasonal dynamics of extremely halophilic microbial communities in
602 three Argentinian salterns. *FEMS Microbiol. Ecol.* 92, fiw184 (2016).

603 15. Javor, B. J. Planktonic standing crop and nutrients in a saltern ecosystem1. *Limnol.*
604 *Oceanogr.* 28, 153–159 (1983).

605 16. Ventosa, A., Fernández, A. B., León, M. J., Sánchez-Porro, C. & Rodriguez-Valera, F. The
606 Santa Pola saltern as a model for studying the microbiota of hypersaline environments.
607 *Extremophiles* 18, 811–824 (2014).

608 17. Harding, T. & Simpson, A. G. B. Recent Advances in Halophilic Protozoa Research. *J.*
609 *Eukaryot. Microbiol.* 65, 556–570 (2018).

610 18. Santos, F., Yarza, P., Parro, V., Briones, C. & Antón, J. The metavirome of a hypersaline
611 environment. *Environ. Microbiol.* 12, 2965–2976 (2010).

612 19. Correa, A. M. S. *et al.* Revisiting the rules of life for viruses of microorganisms. *Nat. Rev.*
613 *Microbiol.* 19, 501–513 (2021).

614 20. Ptashne, M. *A genetic switch: Gene control and phage λ* (Cell Press & Blackwell Scientific
615 Publications, 1986).

616 21. Zeng, L. *et al.* Decision making at a subcellular level determines the outcome of
617 bacteriophage infection. *Cell* 141, 682–691 (2010).

618 22. Hay, I. D. & Lithgow, T. Filamentous phages: masters of a microbial sharing economy.
619 *EMBO Rep.* 20, e47427 (2019).

620 23. Łoś, M. & Węgrzyn, G. Pseudolysogeny. *Adv. Virus Res.* 82, 339–349 (2012).

621 24. Mäntynen, S., Laanto, E., Oksanen, H. M., Poranen, M. M. & Díaz-Muñoz, S. L. Black
622 box of phage–bacterium interactions: exploring alternative phage infection strategies. *Open Biol.*
623 11, 210188 (2021).

624 25. Thingstad, T. F. Elements of a theory for the mechanisms controlling abundance, diversity,
625 and biogeochemical role of lytic bacterial viruses in aquatic systems. *Limnol. Oceanogr.* 45, 1320–
626 1328 (2000).

627 26. Weitz, J. S., Beckett, S. J., Brum, J. R., Cael, B. B. & Dushoff, J. Lysis, lysogeny and
628 virus–microbe ratios. *Nature* 549, E1–E3 (2017).

629 27. Villamor, J. *et al.* Characterization of ecologically diverse viruses infecting co-occurring
630 strains of cosmopolitan hyperhalophilic Bacteroidetes. *ISME J.* 12, 424–437 (2018).

631 28. Erez, Z. *et al.* Communication between viruses guides lysis–lysogeny decisions. *Nature*
632 541, 488–493 (2017).

633 29. Luria, S. E. & Delbrück, M. Mutations of bacteria from virus sensitivity to virus resistance.
634 *Genetics* 28, 491–511 (1943).

635 30. Maynard, N. D. *et al.* A Forward-Genetic Screen and Dynamic Analysis of Lambda Phage
636 Host-Dependencies Reveals an Extensive Interaction Network and a New Anti-Viral Strategy.
637 *PLOS Genet.* 6, e1001017 (2010).

638 31. Shi, K. *et al.* Structural basis of superinfection exclusion by bacteriophage T4 Spackle.
639 *Commun. Biol.* 3, 691 (2020).

640 32. van den Berg, B. *et al.* Structural basis for host recognition and superinfection exclusion
641 by bacteriophage T5. *Proc. Natl. Acad. Sci.* 119, e2211672119 (2022).

642 33. Labrie, S. J., Samson, J. E. & Moineau, S. Bacteriophage resistance mechanisms. *Nat. Rev.*
643 *Microbiol.* 8, 317–327 (2010).

644 34. Treptow, N., Rosenfeld, R. & Yarmolinsky, M. Partition of nonreplicating DNA by the par
645 system of bacteriophage P1. *J. Bacteriol.* 176, 1782–1786 (1994).

646 35. Kourilsky, M. Learning Through Advocacy: An Experimental Evaluation of an Adversary
647 Instructional Model. *J. Econ. Educ.* 3, 86–93 (1972).

648 36. Kourilsky, P. Lysogenization by bacteriophage lambda. *Mol. Gen. Genet. MGG* 122, 183–
649 195 (1973).

650 37. Cornett, J. B. Spackle and Immunity Functions of Bacteriophage T4. *J. Virol.* 13, 312–321
651 (1974).

652 38. Shabram, P. & Aguilar-Cordova, E. Multiplicity of Infection/Multiplicity of Confusion.
653 *Mol. Ther.* 2, 420–421 (2000).

654 39. Weitz, J. S. *Quantitative Viral Ecology: Dynamics of Viruses and Their Microbial Hosts*.
655 (Princeton University Press, 2016).

656 40. Łoś, M. *et al.* Effective inhibition of lytic development of bacteriophages λ, P1 and T4 by
657 starvation of their host, *Escherichia coli*. *BMC Biotechnol.* 7, 13 (2007).

658 41. Bryan, D., El-Shibiny, A., Hobbs, Z., Porter, J. & Kutter, E. M. Bacteriophage T4 Infection
659 of Stationary Phase *E. coli*: Life after Log from a Phage Perspective. *Front. Microbiol.* 7, (2016).

660 42. Abedon, S. T. Lysis of lysis-inhibited bacteriophage T4-infected cells. *J. Bacteriol.* 174,
661 8073–8080 (1992).

662 43. Dressman, H. K. & Drake, J. W. Lysis and Lysis Inhibition in Bacteriophage T4: *rV*
663 Mutations Reside in the Holin *t* Gene. *J. Bacteriol.* 181, 4391–4396 (1999).

664 44. Million-Weaver, S. & Camps, M. Mechanisms of plasmid segregation: have multicopy
665 plasmids been overlooked? *Plasmid* 0, 27–36 (2014).

666 45. Basso, J. T. R. *et al.* Genetically similar temperate phages form coalitions with their shared
667 host that lead to niche-specific fitness effects. *ISME J.* 14, 1688–1700 (2020).

668 46. Thyrhaug, R., Larsen, A., Thingstad, T. & Bratbak, G. Stable coexistence in marine algal
669 host-virus systems. *Mar. Ecol. Prog. Ser.* 254, 27–35 (2003).

670 47. Huang, C. *et al.* Isolation, characterization, and application of a novel specific *Salmonella*
671 bacteriophage in different food matrices. *Food Res. Int.* 111, 631–641 (2018).

672 48. Sant, D. G., Woods, L. C., Barr, J. J. & McDonald, M. J. Host diversity slows bacteriophage
673 adaptation by selecting generalists over specialists. *Nat. Ecol. Evol.* 5, 350–359 (2021).

674 49. Han, K. *et al.* Characterization and genome analysis of a novel phage Kayfunavirus TM1.
675 *Virus Genes* 59, 302–311 (2023).

676 50. Tan, D. *et al.* Characterization of *Klebsiella pneumoniae* ST11 Isolates and Their
677 Interactions with Lytic Phages. *Viruses* 11, 1080 (2019).

678 51. Li, Z. *et al.* Characterization and Application of a Lytic Phage D10 against Multidrug-
679 Resistant *Salmonella*. *Viruses* 13, 1626 (2021).

680 52. Yang, Y. *et al.* Development of a Bacteriophage Cocktail to Constrain the Emergence of
681 Phage-Resistant *Pseudomonas aeruginosa*. *Front. Microbiol.* 11, (2020).

682 53. Alexyuk, P. *et al.* Isolation and Characterization of Lytic Bacteriophages Active against
683 Clinical Strains of *E. coli* and Development of a Phage Antimicrobial Cocktail. *Viruses* 14, 2381
684 (2022).

685 54. Los, M., Wegrzyn, G. & Neubauer, P. A role for bacteriophage T4 *rI* gene function in the
686 control of phage development during pseudolysogeny and in slowly growing host cells. *Res.*
687 *Microbiol.* 154, 547–552 (2003).

688 55. Latino, L., Midoux, C., Vergnaud, G. & Pourcel, C. Investigation of *Pseudomonas*
689 *aeruginosa* strain PcyII-10 variants resisting infection by N4-like phage Ab09 in search for genes
690 involved in phage adsorption. *PLOS ONE* 14, e0215456 (2019).

691 56. Ripp, S. & Miller, R. V. The role of pseudolysogeny in bacteriophage-host interactions in
692 a natural freshwater environment. *Microbiology* 143, 2065–2070 (1997).

693 57. Bratbak, G., Egge, J. & Heldal, M. Viral mortality of the marine alga *Emiliania huxleyi*
694 (Haptophyceae) and termination of algal blooms. *Mar. Ecol. Prog. Ser.* 93, 39–48 (1993).

695 58. Shkoporov, A. N. *et al.* Long-term persistence of crAss-like phage crAss001 is associated
696 with phase variation in *Bacteroides intestinalis*. *BMC Biol.* 19, 163 (2021).

697 59. Rodriguez-Valera, F., Ventosa, A., Juez, G. & Imhoff, J. F. Variation of Environmental
698 Features and Microbial Populations with Salt Concentrations in a Multi-Pond Saltern. *Microb.*
699 *Ecol.* 11, 107–115 (1985).

700 60. Bolger, A. M., Lohse, M. & Usadel, B. Trimmomatic: a flexible trimmer for Illumina
701 sequence data. *Bioinformatics* 30, 2114–2120 (2014).

702 61. Bankevich, A. *et al.* SPAdes: A New Genome Assembly Algorithm and Its Applications
703 to Single-Cell Sequencing. *J. Comput. Biol.* 19, 455–477 (2012).

704 62. Noble, R. T. & Fuhrman, J. A. Use of SYBR Green I for rapid epifluorescence counts of
705 marine viruses and bacteria. *Aquat. Microb. Ecol.* 14, 113–118 (1998).

706 63. Santos, F. *et al.* Metagenomic approach to the study of halophages: the environmental
707 halophage 1. *Environ. Microbiol.* 9, 1711–1723 (2007).

708 64. Smith, C. L., Klco, S. R. & Cantor, C. R. Pulsed-field gel electrophoresis and the
709 technology of large DNA molecules. *Genome Anal. Pract. Approach* 41–72 (1988).

710 65. Kropinski, A. M. *Bacteriophages: Methods and Protocols, Volume 3* (Springer, 2018).

711

712

713

714

715

ACKNOWLEDGEMENTS

We warmly thank to Julia Esclapez and Laura Matarredona for their help with the Southern Blot. We thank Cristina López for providing the initial infection curves. This research was supported by the projects "Virhost" CIPROM/2021/006 (PROMETEO 2022, Generalitat Valenciana) and METACIRCLE PID2021-126114NB-C41-C42 (Spanish Ministry of Science and Innovation). R.S.M. received funding for his doctoral thesis from the Spanish Ministry of Science and Innovation PRE2019-087998. R.S.M., F.S. and J.A. are members of the National Excellence Network FAGOMA (RED2022-134837-T). This project was supported, in part, by Simons Foundation Grant 722153 (to J.S.W.) and by the Chaires Blaise Pascal program of the Île-de-France Region (to J.S.W.).

AUTHOR CONTRIBUTIONS

R.S.M., J.S.W., F.S. and J.A. conceived and designed the study. R.S.M. performed the experiments and analyzed the sequences under the inputs and supervision of M.K., F.S., and J.A.. A.A. and J.S.W. designed and implemented the mathematical model. A.A. wrote the code and performed the simulations and statistical analysis. R.S.M. and A.A. drafted the original manuscript. All authors contributed to manuscript final writing and approved the final paper.

DATA AVAILABILITY

The raw files used for mutation analysis were deposited in the NCBI database with BioProject accession ID PRJNA1136859. Raw sequences of the Sanger sequencing of the mutation affecting the sodium/glucose cotransporter can be found in the *Mutations Supplementary Information*

CODE AVAILABILITY

The code used in the study is available via GitHub at:
https://github.com/aranilah/SalruberM1_EM1_recovery/tree/main

ETHICS DECLARATIONS

The authors declare no competing interests.

761 **FIGURES**

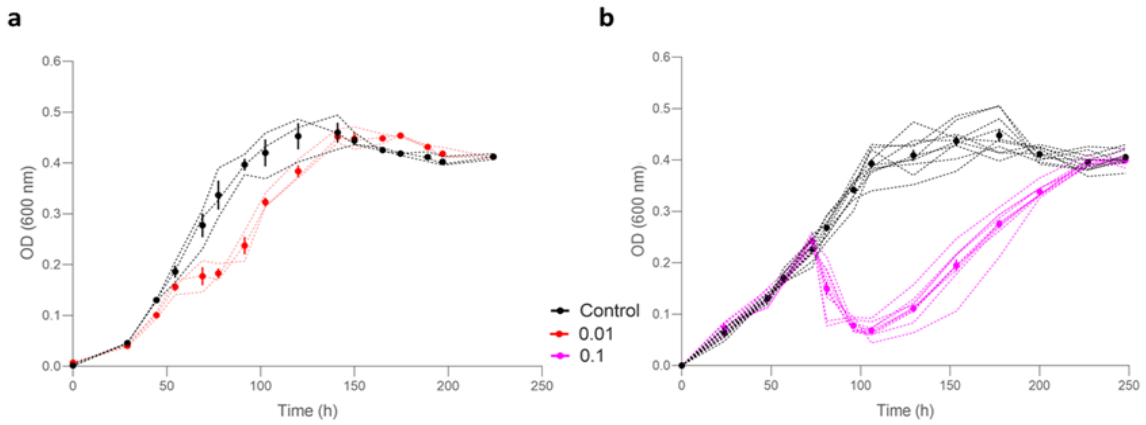

762

763 **Fig. 1**: **Infection experiments showed a reproducible recovery after viral lysis**. Infection
764 experiments of *Sal. ruber* strain M1 with the EM1 virus were performed using two different MOIs.
765 Black lines represent uninfected control and red (**a**, MOI=0.01) and purple (**b**, MOI=0.1) lines
766 represent virus-infected cultures. Each of the individual replicates used are shown as dotted lines.
767 The dots show the mean and the vertical bars the standard error. The experiments were performed
768 with 3 replicates for MOI 0.01 and 10 replicates for MOI 0.1 for both the control and infected
769 cultures. Viruses were mixed with the host at time=0 h.

770

771

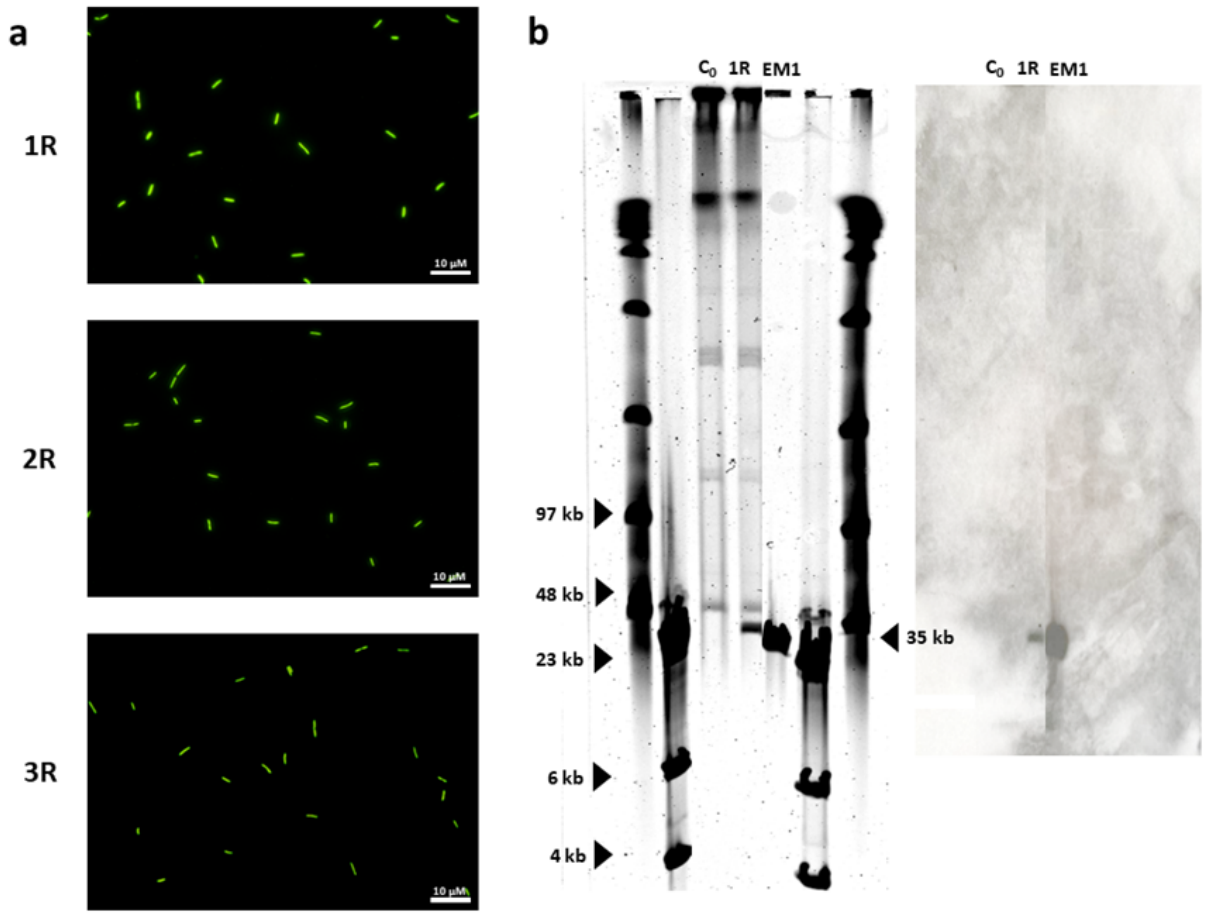

Fig. 2: The EM1 virus establishes a pseudolysogenic state in *Sal. ruber* M1. a, Three randomly selected cultures of the 20 colonies of C_F, PCR positive for the EM1 virus, that we named 1R, 2R and 3R, were stained with SYBR™Gold and observed under epifluorescence microscope to test the presence of extracellular viruses. No extracellular viruses were seen in any of them. 30 fields were examined per sample. The photos shown here are a representation of each sample. Scale bar: 10 µm. **b**, A PFGE was performed (left) comparing initial cells (C_0) with final colony 1R (lines 3 and 4 of the gel, respectively). The DNA of the virus was also loaded as a control (line 5). The PFGE showed a band in 1R with the size of EM1 (35kb) which was not found in C_0. A southern blot (right) with a labeled probe targeting the genome of EM1 confirmed that this band belonged to the virus.

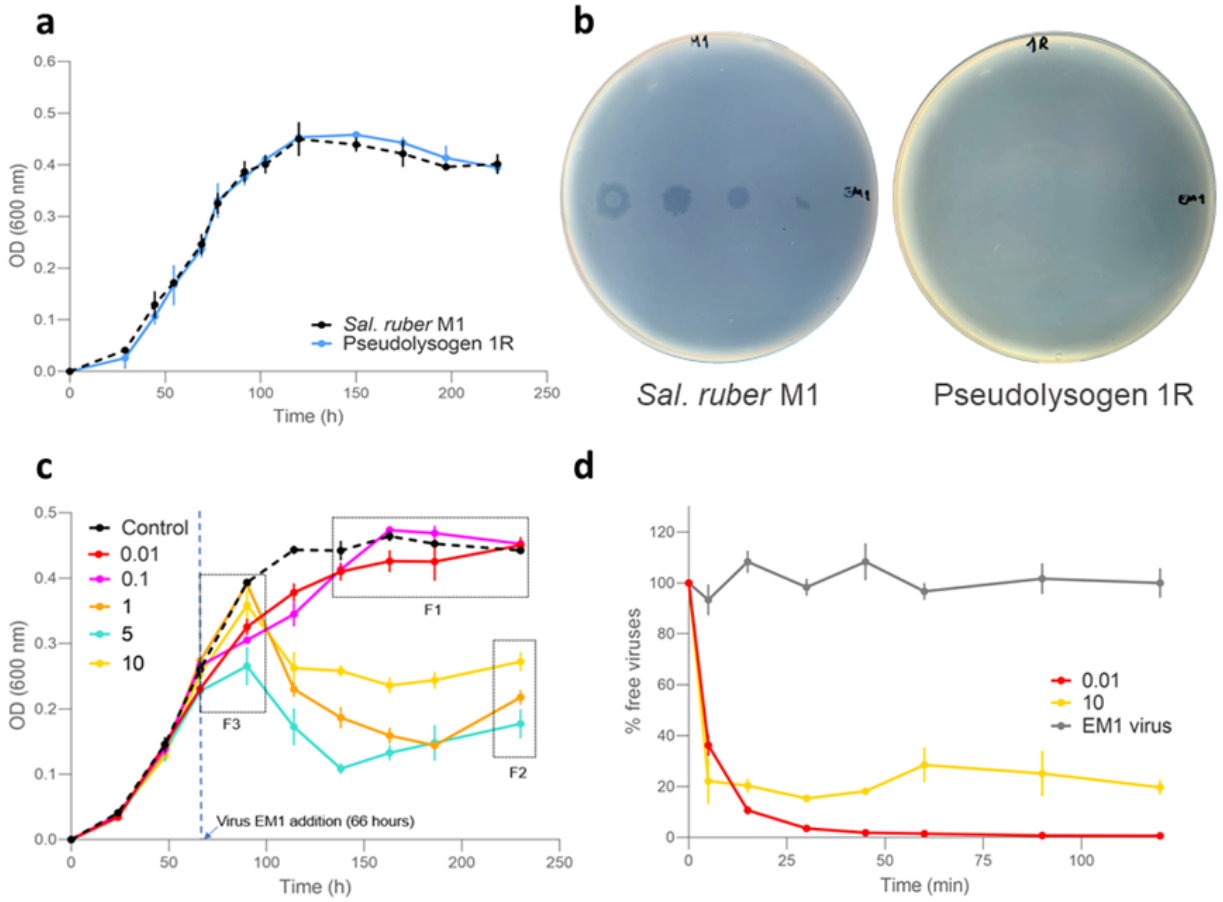

Fig. 3: The acquisition of the virus, which protects *Sal. ruber* M1 of further infections, depends on the MOI. a, Growth curves (performed in triplicate) of *Sal. ruber* M1 wild type (black dotted line) and pseudolysogen 1R (blue line) were performed and their growth dynamics were found to have no statistical differences (*Modeling Supplementary Information: Sal. ruber M1 wild-type and 1R (pseudolysogen) growth comparison*). **b**, Susceptibility to the virus was assessed using a spot test. *Sal. ruber* M1 wild type (left) and pseudolysogen 1R (right) were exposed to 3 µl of the EM1 virus tittered at 10^{10} PFUs/ml (left part of each plate) and diluted 10^2, 10^4 and 10^6 (left to right) times. **c**, Infection curves of *Sal. ruber* M1 and the EM1 virus were performed at different MOI. The M1 cultures were infected at 66 hours, during the exponential growth phase. The black dotted line represents the non-infected control and the different colors indicate the MOI, as is indicated in the legend. The experiment results exhibit three key features (*see text).* **d**, An adsorption assay of the EM1 virus to *Sal. ruber* M1 wild type at MOI 0.01 (red line) and 10 (yellow line), where the number of extracellular viruses (PFU/ml) was measured over 120 minutes. The virus stock used was also set as a decay control (grey line). All the experiments were performed by triplicate. Error bars represent the standard error.

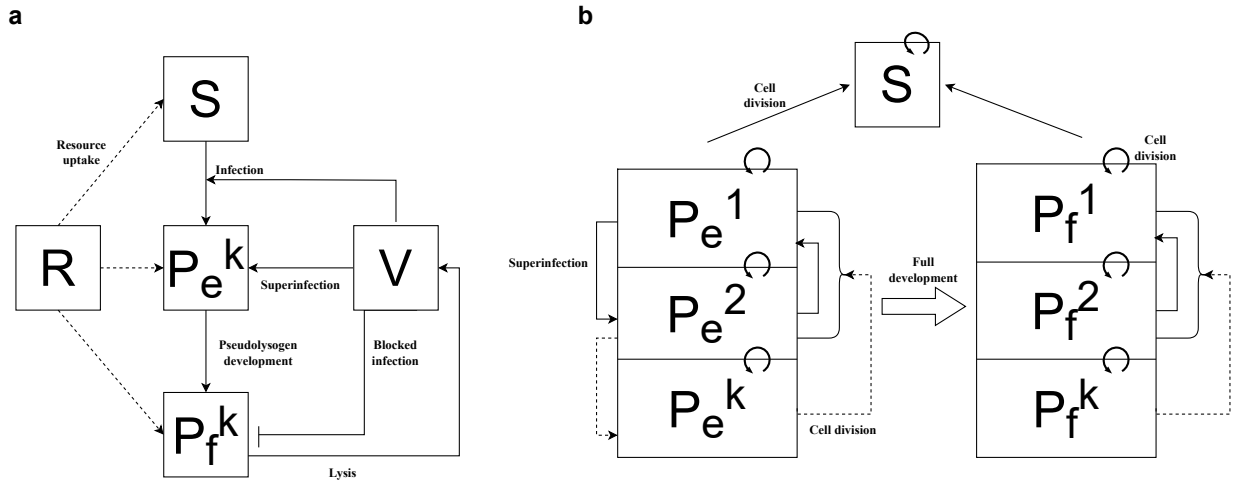

Fig. 4: Schematic of nonlinear dynamics population model of pseudolysogen. a, Schematic representation of the ODE model. R denotes the resource level and V denotes the free virus concentration. The host population is split into three classes: sensitive (S), early pseudolysogen ($P_e{}^k$), and fully developed pseudolysogen ($P_f{}^k$), where k is the number of viral genome copies within the host cell. **b,** Dynamics of pseudolysogen growth and superinfection assuming primary infection has already occurred (primary infection: $S \rightarrow P_e{}^1$). Early pseudolysogens get superinfected causing $P_e{}^k \rightarrow P_e{}^{k+1}$ transitions, while fully developed pseudolysogens are resistant to superinfection at the surface level (denoted by *blocked infection* arrow). Pseudolysogen cell division for both early and fully developed pseudolysogens randomly splits the viral genome of the parent, causing $P^k \rightarrow P^{k\prime}$ transitions where k' is a randomly chosen positive integer that is $\leq k$ (P^0 is virus-free and is therefore equivalent to S). Early stage pseudolysogens eventually transition into fully developed pseudolysogens that still cell divide but are resistant to superinfection.

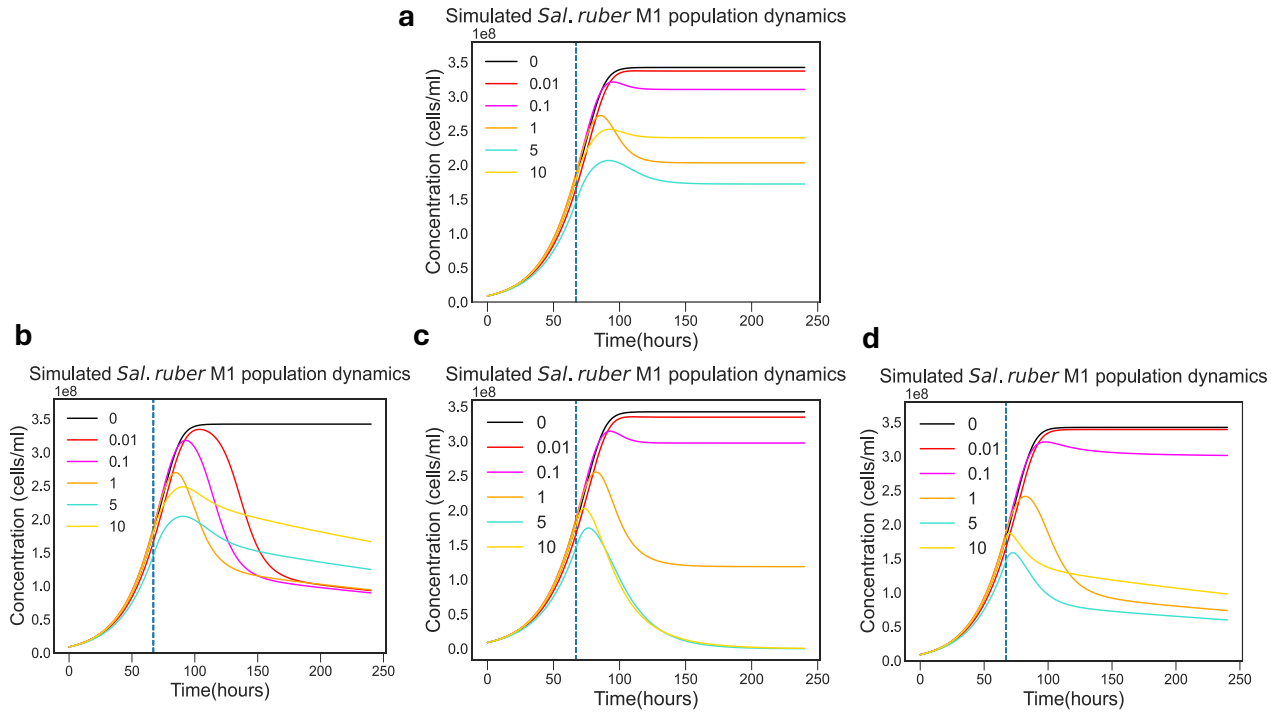

Fig. 5: Theoretical cell division models for pseudolysogens. a, Simulated host population dynamics ($S + \sum_{i=1}^{k} P_e^{[k]} + \sum_{i=1}^{k} P_f^{[k]}$) using the ODE model proposed *(Modeling Supplementary Information: Main Model)* to try and recapitulate the experimental features highlighted in Fig 3c. Subfigures b,c,d graphically show how decoupling features from the model prevents simulations from capturing experimental features. **b,** Simulated host population dynamics with lysis rates independent of resource levels. **c**, Simulated host population dynamics with lysis rates independent of cellular MOI. **d**, Simulated host population dynamics without pseudolysogen cell division.

830 **EXTENDED DATA**

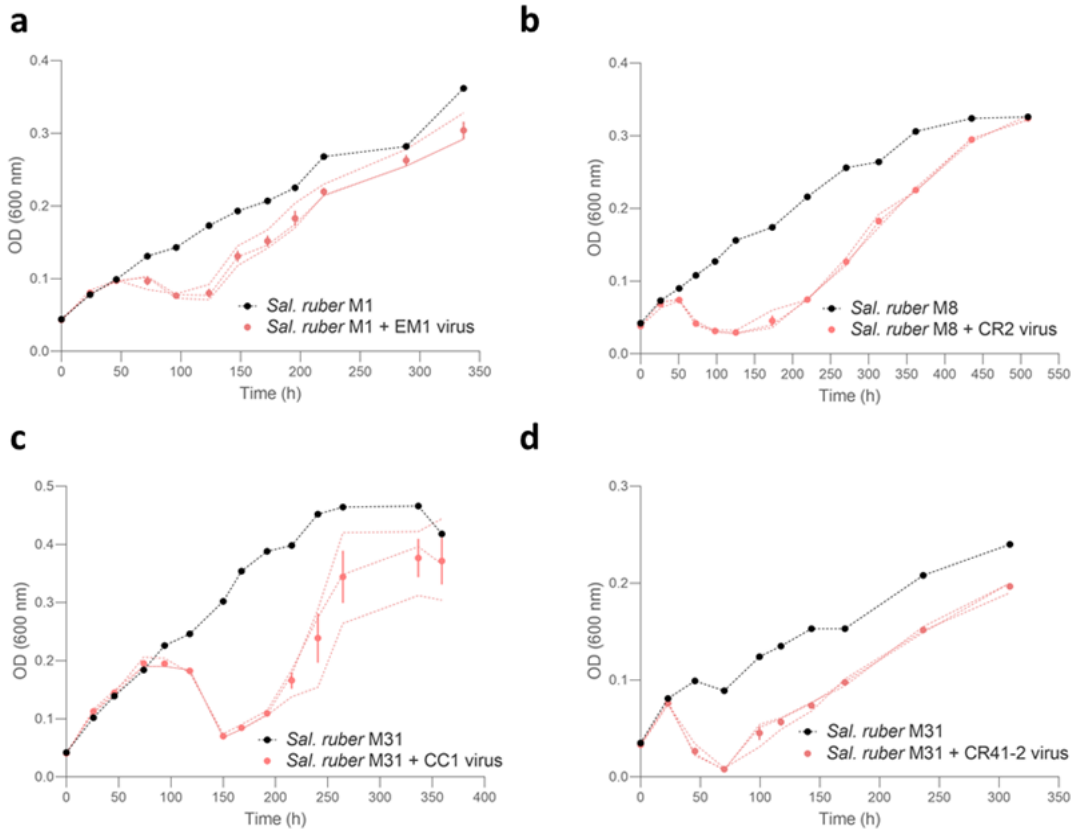

831

832 **Extended Data Fig. 1 Infection curves of different *Sal. ruber* strains and its viruses**. The black
833 dotted line represents the control without viruses and the pink dotted lines represent each replicate
834 of the infected culture. In the infected cultures, the mean is represented by a pink dot and the bars
835 represent the standard error. These curves were made with different strains of *Sal. ruber* and
836 different viruses (**a**, strain M1 and EM1 virus; **b**, strain M8 and CR2 virus; **c**, strain M31 and CC1
837 virus; **d**, strain M1 and CR41-2 virus). The control has only one replicate, while the infection has
838 3 replicates.

839

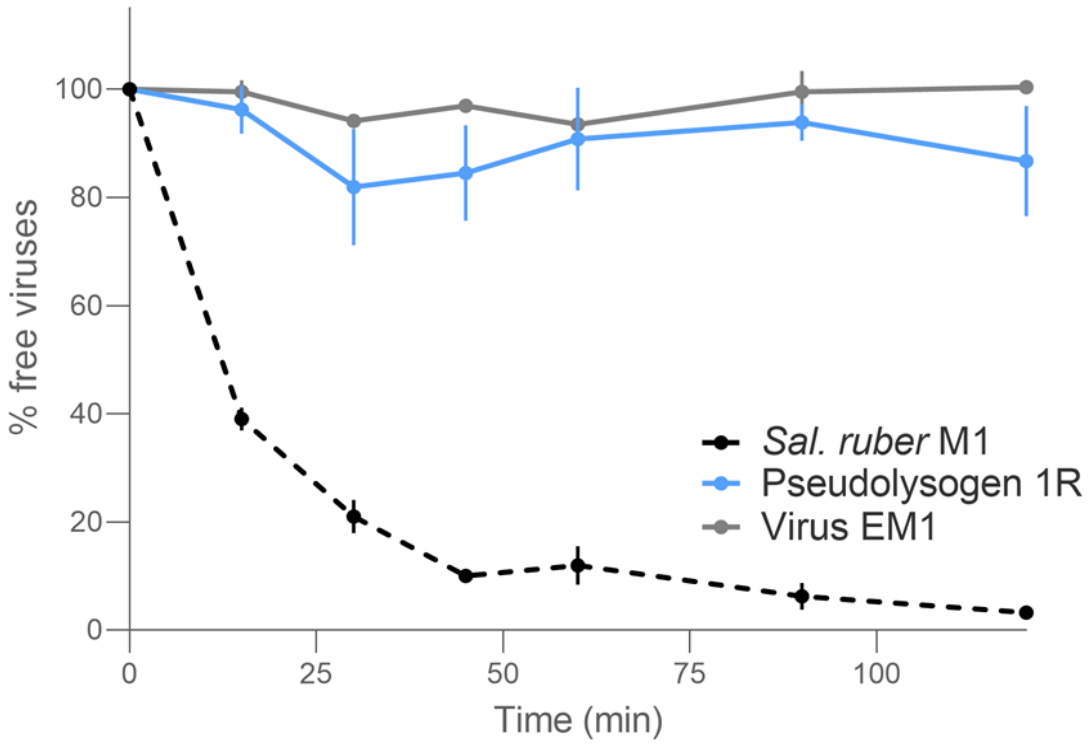

840

841 **Extended Data Fig. 2 Pseudolysogens develop resistance to EM1 at external surface level.** An
842 adsorption assay of the EM1 virus to *Sal. ruber* M1 wild type (black dotted line) and
843 pseudolysogen 1R (blue line) was carried out with a MOI of 0.01, quantifying the quantity of
844 extracellular viruses through PFU/ml during 120 minutes. The experiment was also carried out
845 with the virus alone as a decay control (grey line). The experiment was performed by triplicate.
846 Error bars represent the standard error.

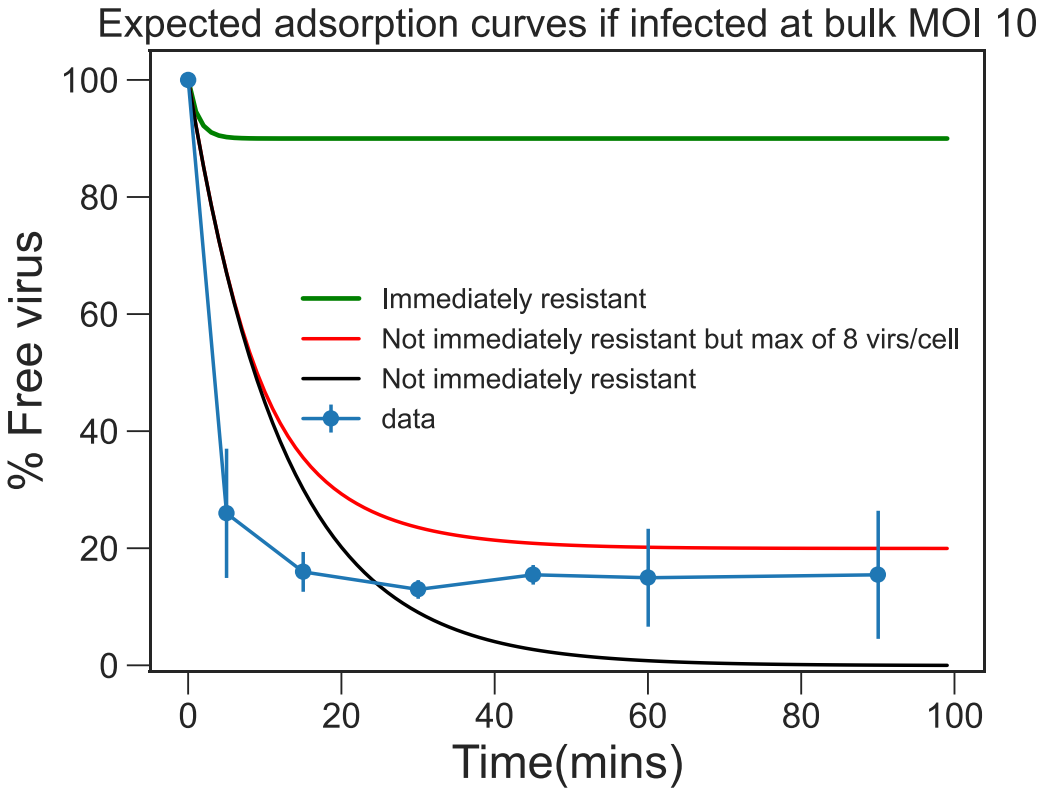

Extended Data Fig. 3 Expected adsorption results with superinfection. The simulated adsorption dynamics when only a single virus can infect a cell (*k=1, green)*, when eight viruses at maximum can infect a cell *k= 8* viruses (*k=8, red*), and when viruses can continuously infect a cell with no limit (*black*). The dynamics when *k=8* seem to match the experimental adsorption dynamics observed in Figure 3d. In reality, the reasoning behind the limit to the number of viruses per cell could be due to competition for receptor sites, or perhaps explicit spatial limitations.

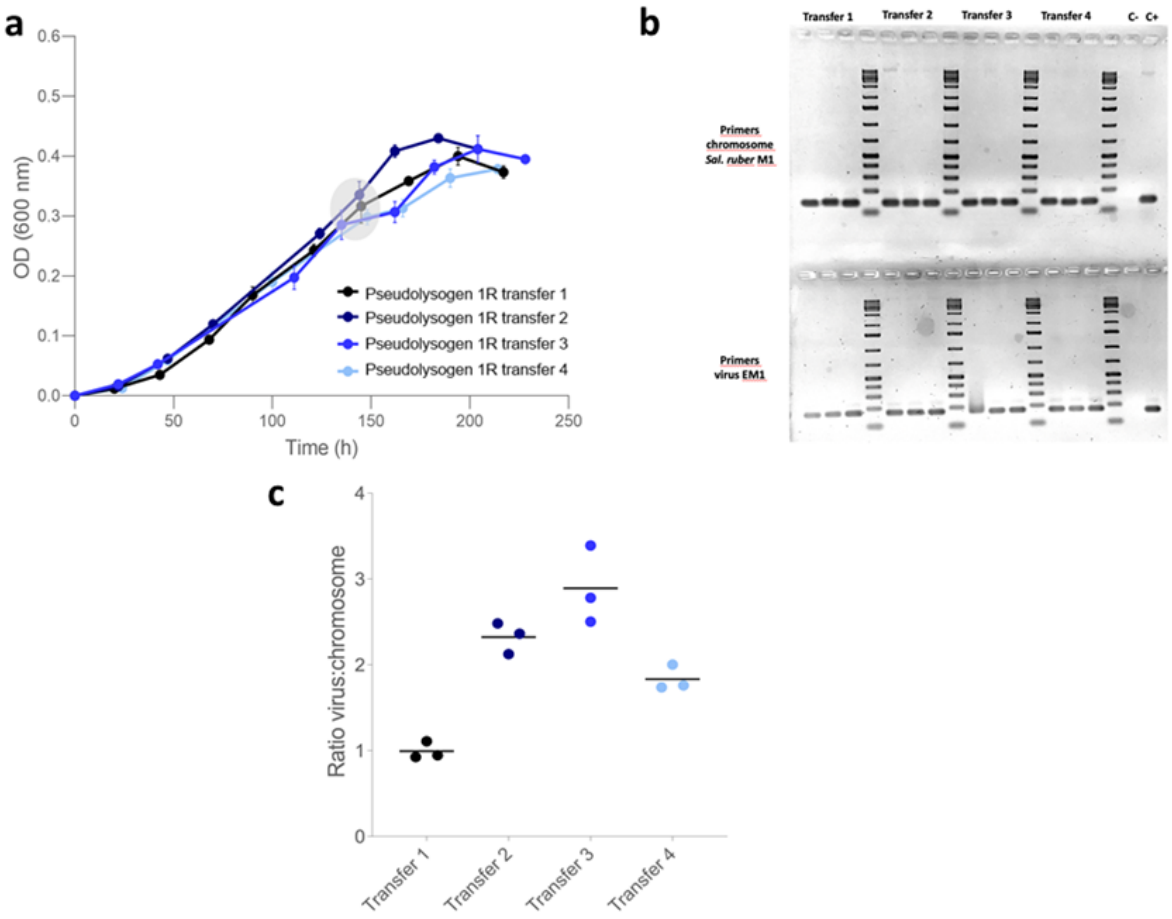

Extended Data Fig. 4 The EM1 virus is maintained at the population level across time. a, Growth curves of the different transfers of pseduolysogen 1R. The points taken for new transfers, spot tests, PCR and qPCR are marked with a grey oval. It was transferred by triplicate. Error bars represent the standard error of the replicates. **b**, PCR of the three replicates of the transfers of pseudolysogen 1R shown above. The PCR was performed with primers for *Sal. ruber* M1 (upper part) and the EM1 virus (bottom part). **c**, qPCRs were performed on each of the 4 transfers to quantify the ratio of EM1 virus genome/chromosome of *Sal. ruber* M1 in the culture. Biological replicates are represented with dots. The mean is represented as a horizontal line.

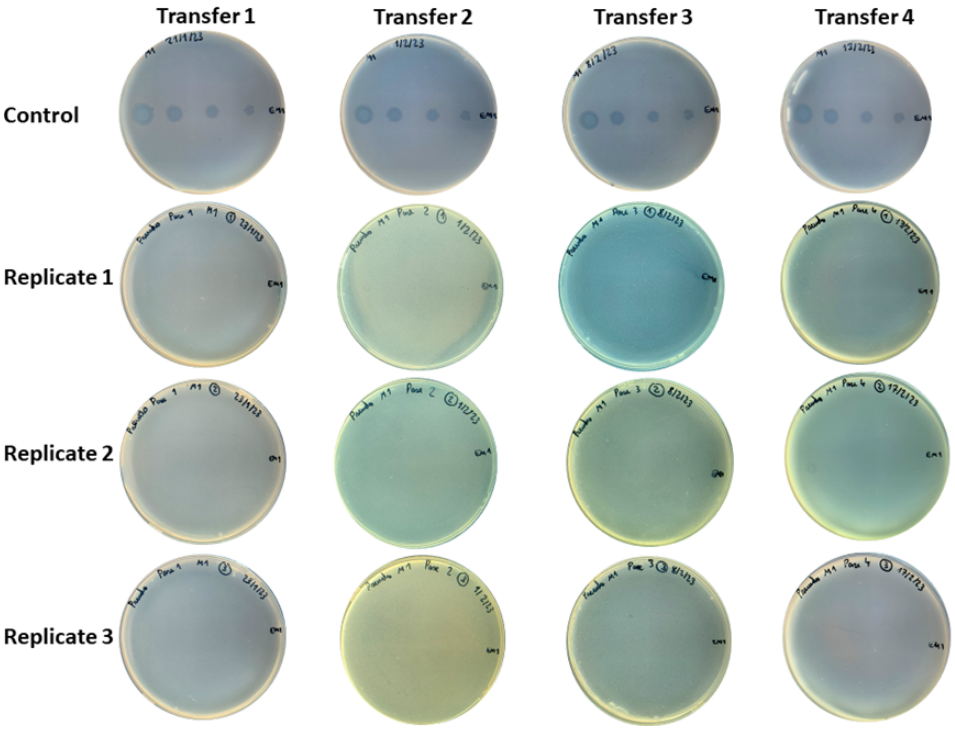

Extended Data Fig. 5 Resistance to the EM1 virus is also maintained over time in the pseudolysogens. Spot tests of the three replicates of the transfers of pseudolysogen 1R to assess the susceptibility to the EM1 virus. All the transfers of pseudolysogen 1R were plated in solid medium and exposed to spots of the EM1 virus tittered at 10^{10} PFUs/ml and diluted 10^2, 10^4 and 10^6 times. A control of *Sal. ruber* M1 wild type (upper part) was included in each transfer to test the infectivity of the virus.

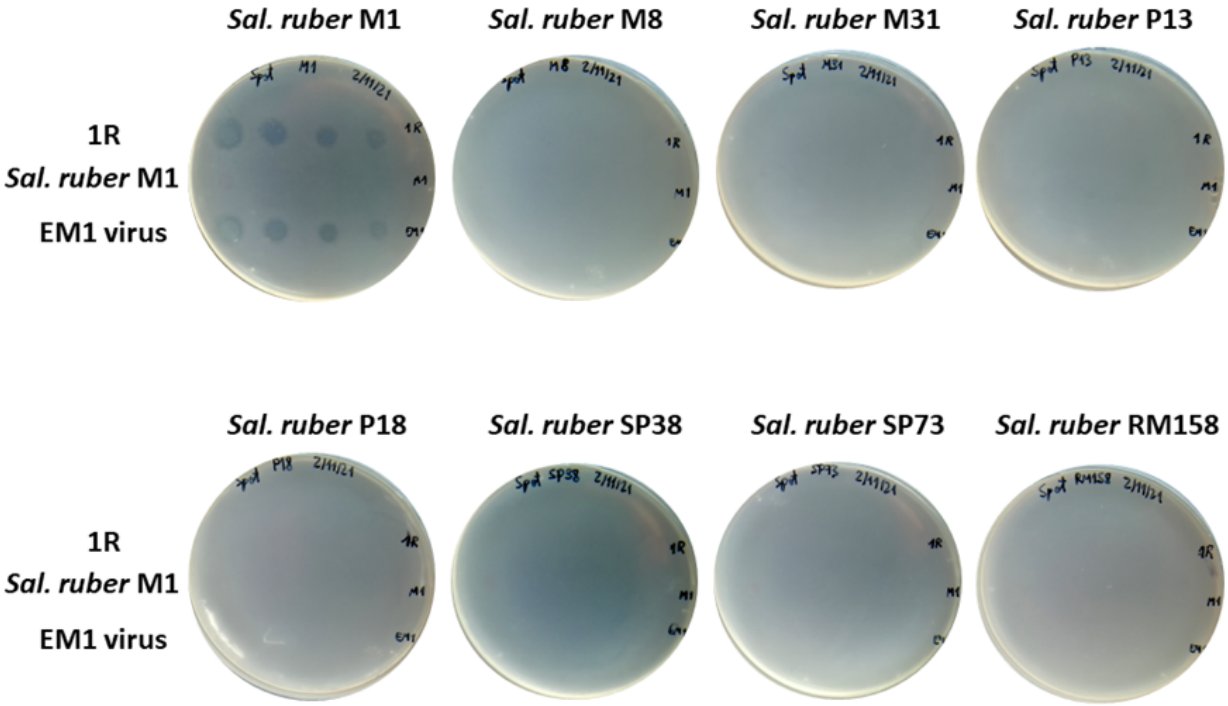

Extended Data Fig. 6 Pseudolysogens kill other virus-susceptible strains. Spot test of eight wild type strains of *Sal. ruber* against the pseudolysogen 1R. All the cultures were plated in solid medium and exposed to spots of pseudolysogen 1R diluted 10^0, 10^2, 10^4 and 10^6 times. Spots of *Sal. ruber* M1 wild type and the EM1 virus were also added as a control.